Wear 484-485 (2021) 204046

Contents lists available at ScienceDirect

Wear

journal homepage: www.elsevier.com/locate/wear

Mechanical and tribological properties of Si and W doped diamond like carbon (DLC) under dry reciprocating sliding conditions

Mingwen Bai [a,c,*], Liuquan Yang [b], Jiayu Li [a], Lun Luo [a], Shikuan Sun [a,d], Beverley Inkson [a,**]

[a] Department of Materials Science and Engineering, The University of Sheffield, Sheffield, S1 3JD, UK
[b] Institute of Functional Surfaces, University of Leeds, Leeds, LS2 9JT, UK
[c] Institute for Future Transport & Cities, Coventry University, Coventry, CV1 5FB, UK
[d] School of Material Science and Energy Engineering, Foshan University, Foshan, 528000, China

ARTICLE INFO

Keywords:
Diamond like carbon
Doping
Thin film
Friction
Wear
Reciprocating

ABSTRACT

The mechanical and tribological properties of three types of diamond like carbon (DLC) coatings, i.e., non-doped, Si-doped, and W-doped DLC, are evaluated. Dry reciprocating sliding wear tests were performed to evaluate the effect of sliding frequency/velocity on friction, adhesion, and wear. The degree of graphitization of non-doped and W-doped DLC increases with sliding velocity, which results in a lower coefficient of friction (COF), and a decrease in wear rate. Si-doped DLC, however, exhibits distinct friction behaviour, with increasing COF and severe fluctuations in friction at higher sliding velocities. In Si-DLC frictional heating drives the formation of an oxide-rich tribofilm and large amounts of Si-rich oxide wear debris that are both adhesive and abrasive. The oxide-rich tribofilm, and lack of surface graphitization, result in the severe fluctuations of Si-DLC friction via stick-slip and surface fracture/wear mechanisms, and significantly increased COF and wear rates at higher sliding velocities.

1. Introduction

Solid lubricant coatings have been widely applied in real industrial applications to improve tribological performances of machine components, particularly in conditions such as clean environments, severe load, slow relative velocity between mating surfaces, and high working temperatures where fluid lubricant films cannot be used or formed [1]. Amongst such coatings, diamond-like carbon (DLC) coatings have attracted a lot of interest because of their low friction, high hardness, good wear resistance and protection of the uncoated counter surface [2–4]{Tyagi, 2019 #32}. These advantages make DLC coatings suitable for many tribological applications in mechanical systems to improve efficiency and durability of machine elements, especially for automotive machine components such as valve train tappets, gears, and piston pins [5–8].

To tailor DLC coatings to specific requirements, it is necessary to apply appropriate DLC coatings for specific machine parts. A variety of coating structures such as multiple functional layers, gradient layers, and variations of material composition, doping and thickness, have been introduced to enhance the tribological performance of top DLC layers [9–12]. Fundamental studies to investigate the correlations between tribological characteristics of specific DLC coatings and working conditions (contact pressure, sliding velocity, rolling condition, lubrication condition, etc.) are required to predict the tribological behaviour of DLC coatings when in use. Many dopants have been used to influence DLCs coating properties; notable dopants include metals, the metalloid Si [13] and non-metal F [14]. Metallic dopants, including Ti and W [15], are often used with the aim to increase the surface activity to oil additives, improving coating/substrate adhesion and altering carbon bonding within the DLC [1].

Si doping of DLC is generating much interest as its inclusion can positively affect the friction coefficient of the coating [16–19], alter the sp^2/sp^3 ratio of the coating, and increase adhesion of the coating to the substrate [20]. A study by Kim et al. reported that non-lubricated Si-DLC contacts can have a lower friction coefficient than non-doped DLCs and that the friction coefficient decreases with increasing silicon concentration in the DLC films [16], however, most lubricated Si-DLC test results are not as favourable [21–23]. In most cases, Si-DLC is reported to increase the overall wear of the coating when compared to non-doped DLCs [24,25]. W-DLC also exhibit a higher wear rate compared to

* Corresponding author. Department of Materials Science and Engineering, The University of Sheffield, Sheffield, S1 3JD, UK.
** Corresponding author.
E-mail addresses: mingwen.bai@coventry.ac.uk (M. Bai), beverley.inkson@sheffield.ac.uk (B. Inkson).

https://doi.org/10.1016/j.wear.2021.204046
Received 17 March 2021; Accepted 20 July 2021
Available online 24 July 2021

other a-C:H and a-C type coatings [26,27].

In this study, the mechanical properties and tribological properties of W and Si doped DLC are studied and directly compared with non-doped DLC. Dry reciprocating sliding tests are carried out to determine DLC friction and wear characteristics against alumina counter-bodies under a range of sliding velocities from 1 Hz up to an extremely high frequency of 36 Hz. This aims to evaluate the effect of sliding frequency/velocity on friction, adhesion, and wear, and to investigate if there is a frequency/velocity related transition when the tribological behaviour of Si and W doped DLCs deteriorates. This knowledge will aid the selection of working conditions where it is advantageous to use Si or W doped coatings in real mechanical systems.

2. Experimental

2.1. Coating deposition

AISI 52100 bearing steel disks with a diameter of 30 mm and a thickness of 2 mm were used as substrates for the DLC coatings, which were mechanically polished to a mirror finish (Ra ≈ 0.1 μm), then washed with heptane in an ultrasonic bath for 15 min, wiped by ethanol and stored in a dry chamber prior to coating deposition. An industrial sized and customized Hauzer Flexicoat® 850 Multi-Purpose Platform was used to produce the DLC thin films. Interlayers were deposited for the adhesion of the functional DLC coatings on the steel substrate. For the functional DLC coatings, the non-doped DLC was deposited using acetylene gas by plasma enhanced chemical vapour deposition (PECVD); the Si-doped DLC was deposited using both Hexamethyldisiloxane (HMDSO) and acetylene by PECVD; the W-doped DLC was deposited using both tungsten carbide magnetron sputtering and acetylene by PECVD. The maximum deposition temperature in the chamber did not exceed 200 °C during the coating procedures.

2.2. Coating characterization

The surface and cross-sectional microstructure of the as-deposited coatings were examined using a field emission scanning electron microscope (FEG-SEM) equipped with a focused-ion beam (FIB, Helios NanoLab G3, FEI), and a 3D optical profilometer (Contour GT Bruker, USA). The mechanical properties of the DLC coatings were measured by nanoindentation (TriboScope, Hysitron, USA) using a Berkovich diamond tip at 10 mN load. The indentation contact depth was kept within less than 10 % of the film thickness to obtain the intrinsic film properties with minimal effect from the substrate underneath. The DLC thin films were further examined by Raman Spectroscopy using a Renishaw InVia Raman Microscope with 50x objective at an excitation wavelength of 514 nm at ambient conditions with 2 mW laser power (10 mW for W-DLC due to insufficient signal strength as caused by the rough surface) and 10s exposure time. The three DLC nano-composite coatings are all fully amorphous with no crystalline peaks detected by grazing incidence X-ray diffraction (GIXRD; PANalytical model X'Pert PRO diffractometer, Cu Kα radiation at 1° angle).

2.3. Wear testing

Tribological tests were carried out using a UMT-2 TriboLab (Bruker, USA) at room temperature 20–25 °C, relative humidity 50–60 %, unlubricated, and under ambient atmospheric conditions. Reciprocating sliding tests were conducted in a ball on plate configuration, which conformed to ASTM G133, with the parameters listed in Table 1. The load condition corresponds to an initial Hertzian contact pressure of 700–800 MPa and a maximum shear stress of 200–250 MPa. During the sliding tests, the dynamic COF was recorded as a function of time using the servo-controlled normal load and lateral load on the DFM-0.5 loading cell (0.05–5 N) with a resolution of 0.25 mN. At least three reciprocating tests were conducted at each test condition, and the averaged specific wear rates are reported. The number of repeated tests was determined by the repeatability of the COF measurements, i.e., if the COF varied significantly between two tests, then further repeated measurements were carried out to evaluate the statistical spread.

Table 1
Reciprocating wear tests at variable frequency 1–36 Hz to alter average sliding velocity.

Normal Force	4 N		
Frequency	1 Hz	6 Hz	36 Hz
Stroke length	2 mm		
Number of cycles	108,000		
Total distance	43.2 m		
Average velocity	4 mm/s	24 mm/s	144 mm/s
Test Duration	180min	30min	5min
Counter-body	Al_2O_3 ball (Φ 4 mm, grade 10)		
Test environment condition	Temperature 20–25 °C, Humidity 50–60 %, unlubricated		

2.4. Wear analysis

After DLC wear tests, the wear scars were examined under an optical microscope (Nikon Eclipse E600 POL). Wear volumes were measured from the post-test wear tracks using a 3D optical profilometer (Contour GT Bruker, USA). Average COF and specific wear rate results were statistically analysed by one-way analysis of variance Tukey test in OriginLab software. Statistical significance was reported at p, 0.05 (*), p, 0.01 (**), p, 0.001 (***) and p, 0.0001 (****) unless otherwise stated. The wear debris was analysed using a FEG-SEM (Inspect F50, FEI) and an energy dispersive X-ray spectroscopy (EDX, Oxford Instruments, UK).

3. Results

3.1. Coating characterization

The DLC, Si-DLC and W-DLC coatings were successfully grown by PVD. Fig. 1 shows the cross-sectional microstructure of the three DLC coatings on steel substrates. A thin layer of platinum was deposited on the coatings surface for protection during focused ion beam milling of the cross-sections. The DLC coatings have a multilayer coating architecture, with an underlying 0.3 μm thick Cr adhesive layer and a 0.7 μm a-C:H:W gradient layer (amorphous tungsten-doped hydrogenated carbon, which has similar composition to the W-doped DLC coating in Fig. 1 (c)). Details of the multi-layer structure and layer thickness measurements of the three DLC coatings are listed in Table 2.

The surface topography of the as-fabricated DLC coatings was evaluated using SEM (Fig. 2), and 3D profilometry across a larger area (Fig. 3, note the significant difference in scale bars). All three coatings exhibited shallow cap-shaped bumps, of heights <200 nm, and in-plane widths up to 2 μm (Fig. 2). Si-doped DLC exhibits the smoothest surface with a surface roughness (Sa) of 15.1 nm (Fig. 3 (b)), compared to the non-doped DLC surface roughness Sa = 35.6 nm (Fig. 3 (a)). The W-doped DLC coating exhibited the roughest surface with Sa = 52.6 nm (Fig. 3 (c)) due to coarser micro-bumps on the as-fabricated coatings surface.

Surface mechanical properties of the three DLC coatings were analysed by nanoindentation at 10 mN load (Fig. 4). The contact depths of all measurements were less than 10 % of each coating thickness to avoid influence of the steel substrate (Fig. 4 (a, b)). The average reduced modulus (Er) of the three coatings is similar, within the range of 140–160 GPa. The average hardness (H) decreases from 22 GPa in the pure DLC coating down to 16 GPa for Si and 13 GPa for W doped DLC (Fig. 4(c)), resulting in the same decreasing trend for the H/Er ratio (Fig. 4(d)). The scatter of Er and H is seen to be higher for W-DLC than for DLC and Si-DLC, likely related to it having the roughest coating surface (Sa = 52.6 nm) covered in micro-bumps. The W-DLC surface

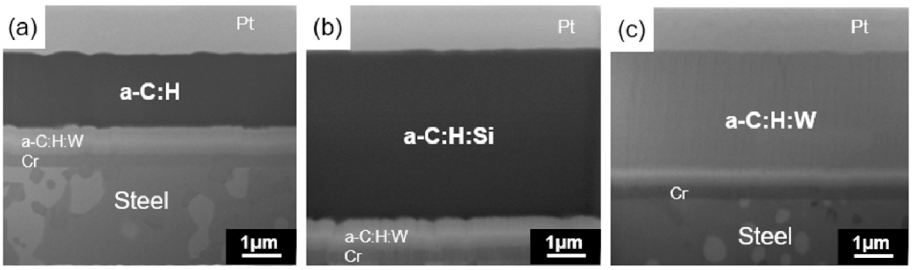

Fig. 1. Cross-sectional SEM imaging of the as-fabricated DLC coatings on the steel substrates with Cr interlayer and a-C:H: W gradient layer: (a) DLC; (b) Si-DLC; (c) W-DLC.

Table 2
DLC multilayer coating architecture with layer thickness measurement.

	DLC	Si-DLC	W-DLC
DLC layer (μm)	1.9	4.2	3.0
Adhesive Cr layer (μm)	0.3	0.3	0.3
Gradient W–C:H layer (μm)	0.7	0.7	–
Coating total thickness (μm)	2.9	5.2	3.3

micro-bumps result in the widest range of contact conditions, with indent depths at 10 mN load ranging from 100 nm to 200 nm, and lateral indent sizes of 1–2 μm that extend over a few bumps on the surface.

3.2. DLC friction coefficients

The variation of COF with sliding velocity was investigated for the doped and undoped DLC coatings. Fig. 5(a–c) show typical variations of friction coefficients of DLC, Si-DLC and W-DLC coatings as a function of number of cycles at reciprocating frequencies of 1 Hz, 6 Hz and 36 Hz. For non-doped DLC (Fig. 5(a)), the COF stablized quickly after the initial run-in period and then remained almost constant for a given frequency during the entire sliding distance, and lower COF occurred for the higher sliding velocities. For Si-doped DLC (Fig. 5(b)), the measured COF is stable at 1 Hz, however severely fluctuated at 6 Hz and 36 Hz reciprocating frequencies, with more frequent and larger COF spikes at 6 Hz than 36 Hz. For W-doped DLC (Fig. 5(c)), the COF is relatively more stable at 1 Hz and 36 Hz than at 6 Hz, which for the analysed sample shows a nearly 50 % drop of COF after ~2000 cycles. This transition of COF to lower values was observed in all W-doped DLC samples tested at 6 Hz.

To quantitatively analyse the frictional behaviour of the different coatings as a function of sliding frequencies, average COF values were calculated over 0–108,000 cycles from three repeated reciprocating wear tests for each coating and frequency. Fig. 6 shows the dependence of average COF on reciprocating test frequency. Error bars indicate the spread of average COF values among all tests under identical conditions, and the asterisks on the top of two chosen columns indicate the confidence interval for the difference between the two means.

Non-doped and W-doped DLC show a trend of decreasing COF at higher frequencies (Figs. 5 and 6). In particular, the average COF of W-DLC significantly decreases from 0.18 at 1 Hz, to 0.13 at 6 Hz and 0.09 at 36 Hz. For non-doped DLC, the drop of COF is not significant from 1 Hz to 6 Hz within the range of 0.08–0.10, however at 36 Hz the COF significantly drops to 0.05. In contrast, however, the average COF of Si-DLC show the opposite trend, increasing with sliding frequency/velocity, namely COF 0.05–0.06 at 1 Hz and 6 Hz significantly rising to 0.13 at 36 Hz.

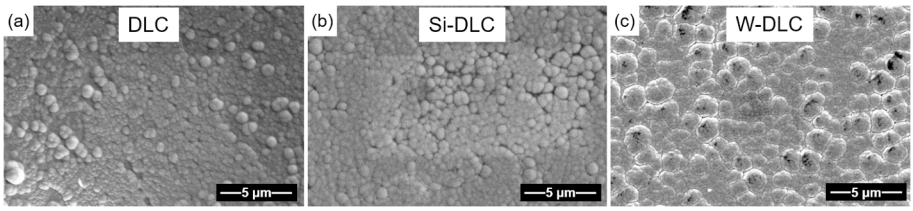

Fig. 2. Surface SEM imaging of the as-fabricated coatings: (a) DLC, (b) Si-DLC and (c) W-DLC.

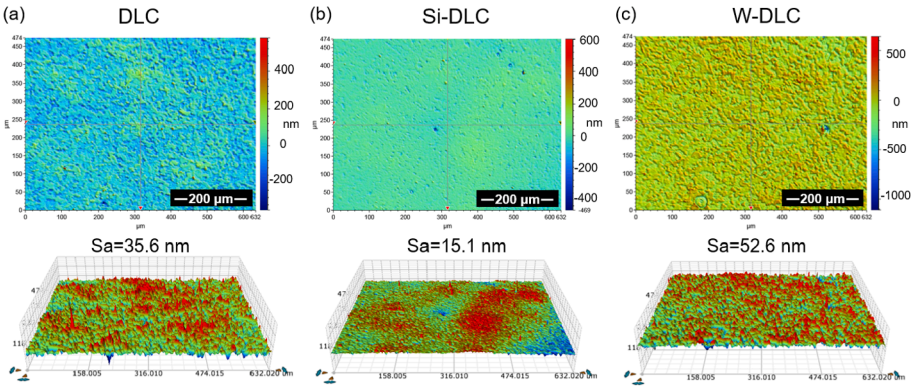

Fig. 3. Surface topography of the as-fabricated coatings: (a) DLC, (b) Si-DLC and (c) W-DLC imaged by 3D profilometry on a wider scale (note the significant difference in scale bar with SEM).

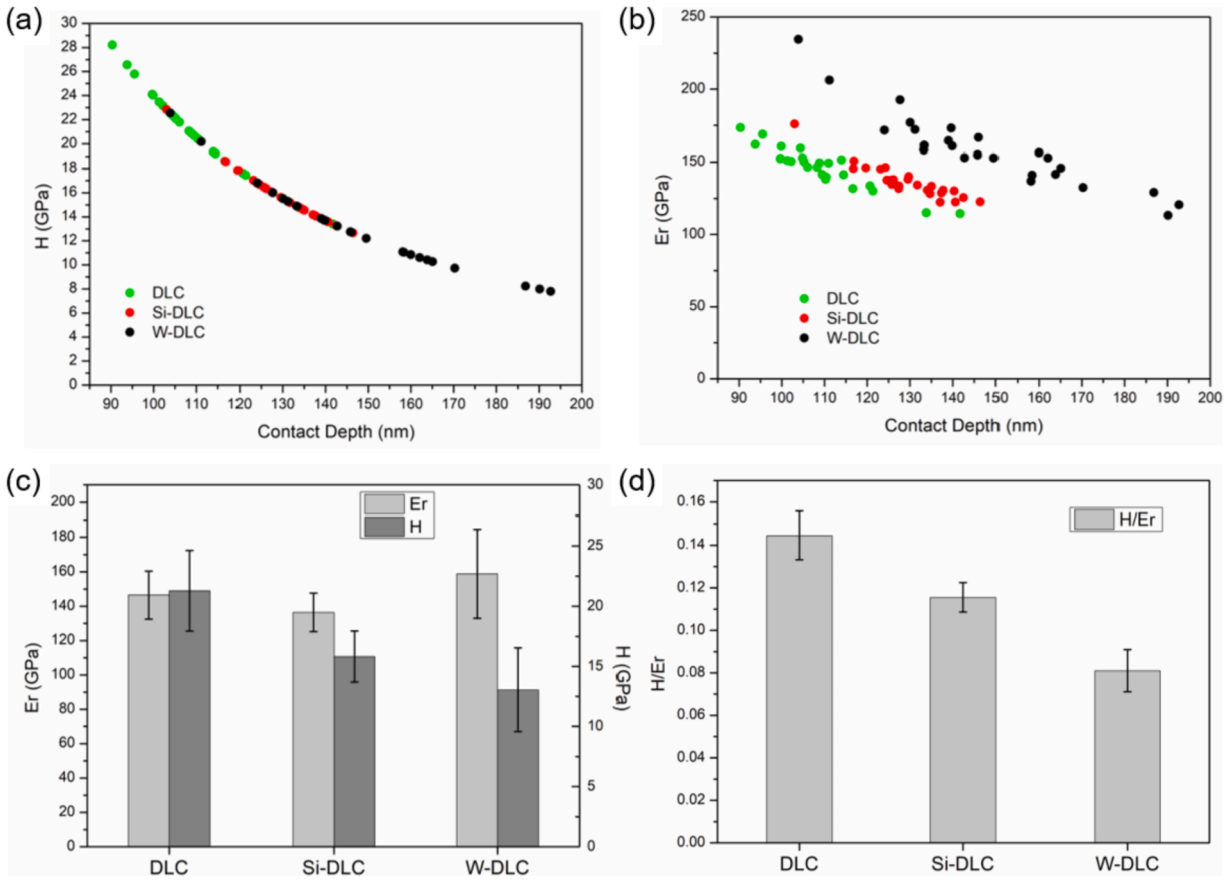

Fig. 4. Mechanical properties of the DLC, Si-DLC, and W-DLC coatings measured by nanoindentation at a normal load of 10 mN. (a) Hardness (H) and (b) Reduced Modulus (Er) as a function of indentation contact depth; and plot of (c) Average Er and H; and (d) Average H/Er ratio.

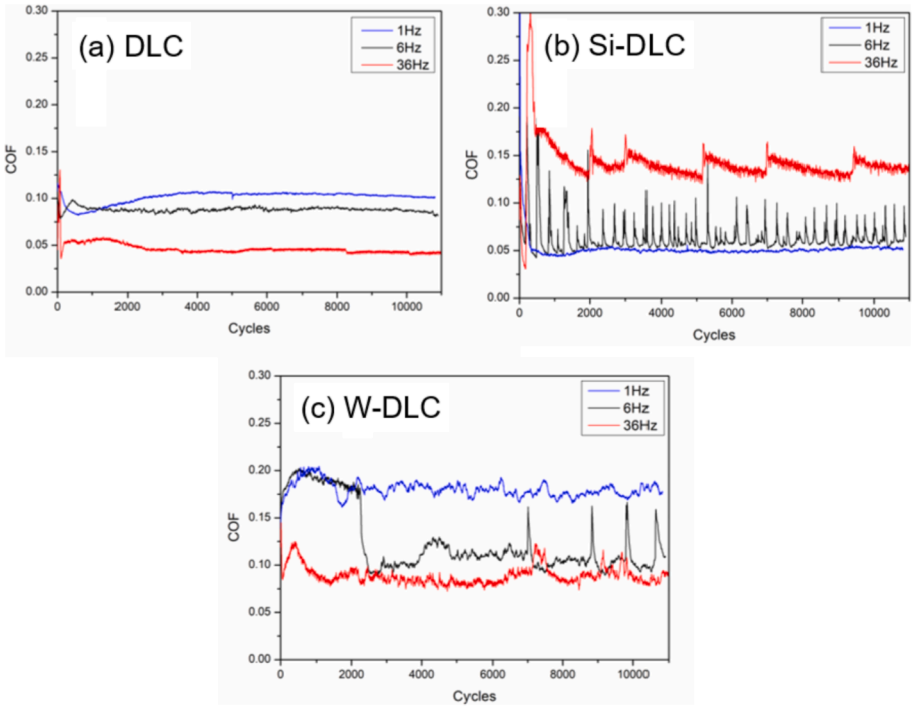

Fig. 5. Coefficient of friction (COF) measurements of the DLC, Si-DLC, and W-DLC coatings as a function of number of reciprocating cycles at different reciprocating frequencies: 1 Hz, 6 Hz and 36 Hz, at 4 N load and 2 mm stroke length with an Al_2O_3 counter-ball: (a) DLC, (b) Si-DLC, and (c) W-DLC.

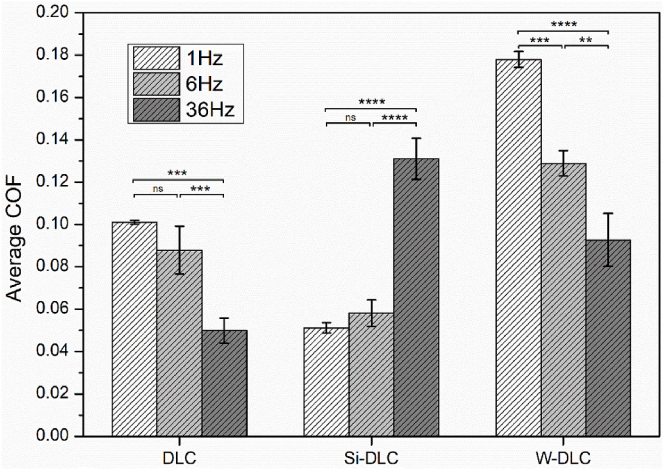

Fig. 6. Dependence of the COF friction of the DLC, Si-DLC, and W-DLC coatings on reciprocating frequency (1 Hz, 6 Hz and 36 Hz), with average COF values each obtained from three repeated tests over 0–108,000 cycles. Asterisks indicate a statistical difference (*p < 0.05, **p < 0.01, ***p < 0.001, ****p < 0.0001, as obtained using Tukey test, which computes a confidence interval for the difference between two means).

3.3. DLC specific wear rate

Fig. 7 shows the dependence of the specific wear rates of the DLC, Si-DLC and W-DLC coatings on the reciprocating sliding frequency. The specific wear rate rank order is non-doped DLC < Si-DLC < W-DLC at 1 Hz and 6 Hz. However, at 36 Hz Si-DLC has a substantial increase in wear rate whilst W-DLC drops. This increase in Si-DLC's wear rate with sliding frequency accompanies the significant increase of measured COF at 36 Hz (Fig. 6). For non-doped DLC, there is no significant difference of the specific wear rates at the three investigated frequencies. While Si-DLC shows a trend of increasing wear at higher frequencies, and W-DLC shows a mixed trend, with the highest wear rate at the intermediate 6 Hz frequency.

3.4. Reciprocating wear tracks

The reciprocating wear tests cause localised surface damage to the DLC coatings, and the wear-scars were examined by optical microscopy and SEM. Figs. 8–10 show the surface morphology of the DLC, Si-DLC and W-DLC coatings after dry reciprocating wear tests (4 N, total distance 43.2 m and frequencies of 1 Hz, 6 Hz and 36 Hz), together with the associated wear of the counter-face Al_2O_3 balls (the reciprocating direction marked by the white arrow). For the undoped DLC, occasional spalled areas occurred within the wear tracks, exposing the adhesive/gradient layer (Fig. 1) and substrate underneath (Fig. 8(d and e)). The fracture of the undoped DLC indicates the coatings' brittleness, with low fracture toughness. Fig. 8 (f) shows typical submicron size wear debris particles that were found accumulating in the vicinity of spall scars, whilst larger wear debris particles distributed around the edges of the main wear scars.

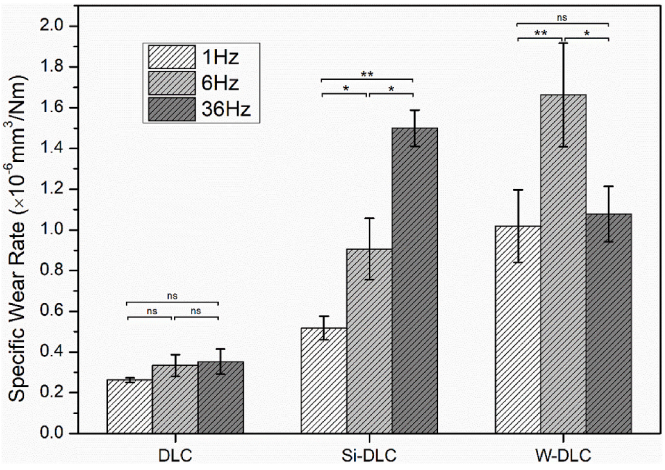

Fig. 7. Dependence of the specific wear rate of the DLC, Si-DLC, and W-DLC coatings on reciprocating frequency (1 Hz, 6 Hz and 36 Hz), with specific wear rates obtained from three repeated tests. Asterisks indicate a statistical difference (*p < 0.05, **p < 0.01, ***p < 0.001, ****p < 0.0001, as obtained using Tukey test, which computes a confidence interval for the difference between the two means).

The Si-DLC coatings tested at three different frequencies: 1 Hz, 6 Hz and 36 Hz exhibited smooth wear tracks and surrounding wear debris (Fig. 9). The amount of wear debris formed on the surface and counter-face ball significantly increased with sliding frequency 1 Hz–36 Hz (Fig. 9(a–c)). Fig. 9(d–f) show the typical sub-micron particle morphology of the wear debris that was formed on the Si-DLC at 6 Hz. The wear debris was distributed around the entire wear track, with a higher volume deposited at the two ends of the reciprocating tracks.

Significant wear and debris were also found on the W-DLC (Fig. 10) compared to the non-doped DLC (Fig. 8). Notably, the W-DLC wear tracks also exhibit deep grooves at all three test different frequencies (Fig. 10(a–c)), indicating an abrasive wear mechanism against the Al_2O_3 counter-body balls, which have also been severely worn and abraded. Wear debris around the wear tracks is seen in the form of sub-micron particles (Fig. 10(f)). In addition, a network of cracks is observed at the bottom of the wear-tracks (Fig. 10 (e)) that appear to preferentially propagate along the boundaries of the original coarse surface bumps of the W-DLC (Fig. 3 (c)).

Fig. 11 shows representative line profiles of the topography of the wear tracks on the DLC coatings, taken in cross-section perpendicular to the reciprocating sliding direction. The depths of all wear tracks are within the DLC coatings thickness (Table 2, DLC: 1.9 μm, Si-DLC: 4.2 μm and W-DLC: 3.0 μm), confirming that the coatings are not worn down to the adhesive and gradient layers underneath the DLC after the wear test (total distance 43.2 m). The wear tracks on both non-doped DLC and Si-DLC coatings exhibit minimal lateral pileups (<0.2 μm), whereas the wear tracks on the higher wear-rate W-DLC show up to 1 μm pileup at both scratch edges (Fig. 11(c)). After reciprocating wear tests, wear debris is also found on the Al_2O_3 balls slid against both Si-DLC and W-DLC, with more debris on the latter, whilst nearly no debris is seen on the ball slid against non-doped DLC (Figs. 8–10). The quantity of debris surrounding the ball wear scars is higher along the linear reciprocating direction, particularly for the W-DLC tests (Fig. 10). The Al_2O_3 balls rubbed against non-doped DLC and Si-DLC showed minimal wear scars, corresponding to specific wear rates in the order of 10^{-9} to 10^{-10} mm^3/Nm, which are significantly lower than the associated wear rates of the investigated DLC coatings. For the Al_2O_3 ball rubbed against Si-DLC, the wear scar becomes clearly larger at 36 Hz as compared to 1 Hz and 6 Hz. The Al_2O_3 balls rubbed against W-doped DLC show larger wear scars, corresponding to specific wear rates in the order of 10^{-8} to 10^{-9} mm^3/Nm.

The chemical composition of the wear debris adjacent to wear tracks on the Si-DLC and W-DLC after the 36 Hz wear test (Si-DLC wear rate 1.5×10^{-6} mm^3/Nm; W-DLC wear rate 1.05×10^{-6} mm^3/Nm) was analysed by EDX spectroscopy (Fig. 12). Carbon is detected across the analysed areas, which comprise large <3 μm debris particles on substrate for Si-DLC (Fig. 12(a)), and smaller <1 μm particles for W-DLC (Fig. 12(b)). There is a clear reduction in carbon K_α X-rays signal in the locations of large debris particles, due to both the particle chemistry and the underlying DLC substrate having a reduced contribution to the X-ray signal. The wear debris on the Si-DLC coatings (Fig. 12(a)) is primarily oxide, with a significant aluminium content (from the wear of the counter-face balls). In comparison the debris on the W-DLC is also oxide,

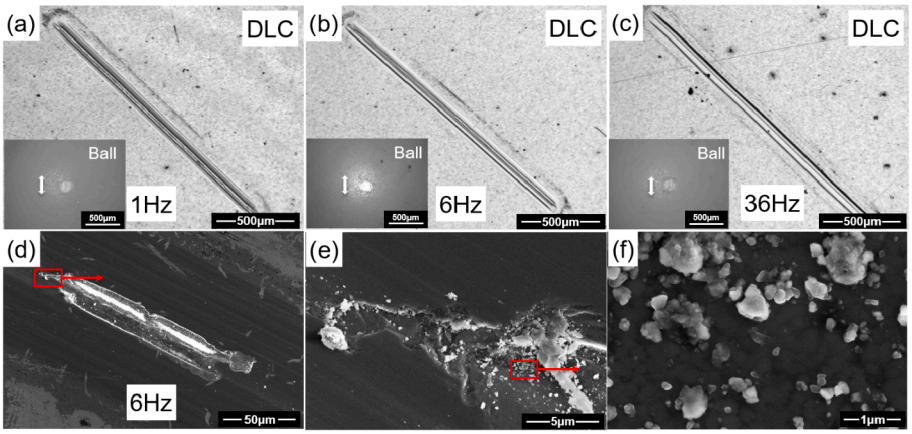

Fig. 8. Surface optical imaging of typical wear tracks on non-doped DLC coatings after 4 N wear tests at (a) 1 Hz; (b) 6 Hz; (c) 36 Hz; with inset showing wear of the counter-face Al_2O_3 balls (the reciprocating direction marked by the white arrow). (d, e) SEM imaging of spalled area within the 6 Hz wear track, and (f) wear debris found in the fractured area under higher magnification.

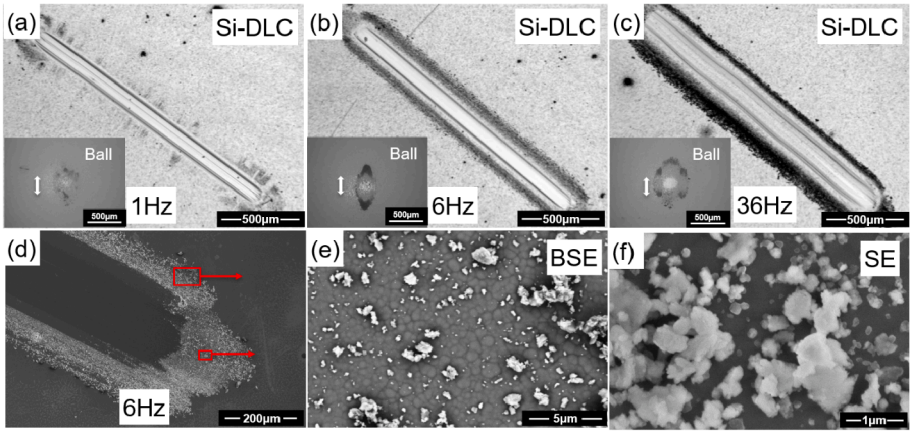

Fig. 9. Surface optical imaging of typical wear tracks on Si-DLC coatings after 4 N wear tests at (a) 1 Hz; (b) 6 Hz; (c) 36 Hz; with inset showing wear of the counter-face Al_2O_3 balls (the reciprocating direction marked by the white arrow). (d–f) SEM imaging of wear debris distributed around the edge of the 6 Hz wear track.

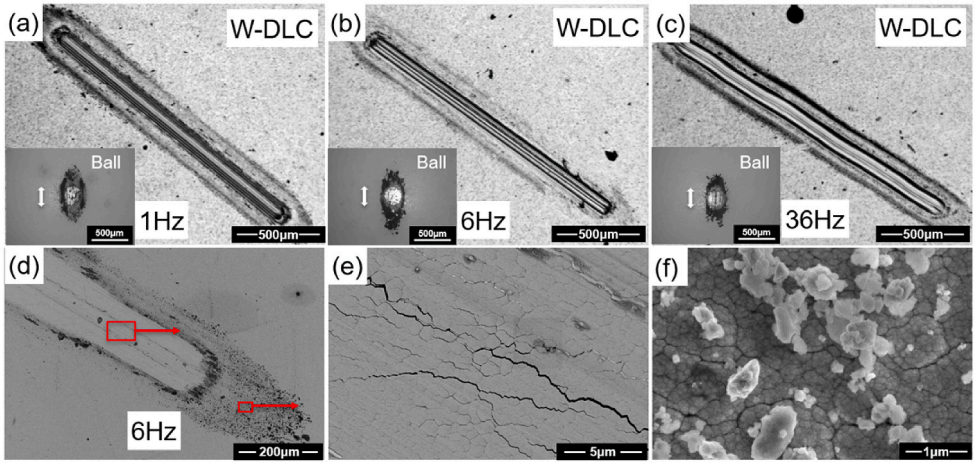

Fig. 10. Surface optical imaging of typical wear tracks on W-DLC after 4 N wear tests at (a) 1 Hz; (b) 6 Hz; (c) 36 Hz; with inset showing wear of the counter-face Al_2O_3 balls (the reciprocating direction marked by the white arrow). (d–f) SEM imaging of a 6 Hz wear track with (e) cracking along the base of the wear-scar, and (f) wear debris deposited beyond the end of the wear track with surface cracking of the underlying coating.

containing tungsten, but with a reduced aluminium (<0.1 wt%) content.

To examine changes to the DLC coatings with friction and wear, laser Raman spectroscopy of the DLC coatings was carried out. Raman spectra obtained from the DLC coatings surface can be decomposed into D (disorder) and G (graphite) bands by Gaussian peak separation method [28], and factors related to the D and G bands were used to estimate the

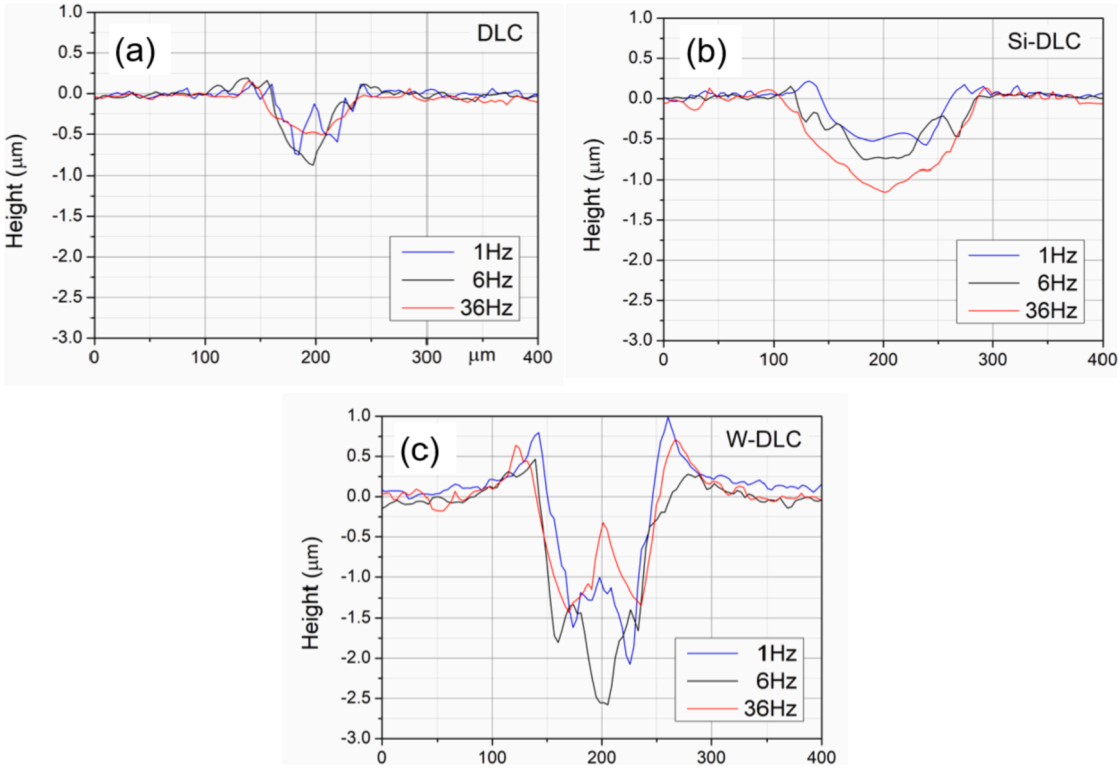

Fig. 11. Line profiles of the topography of the wear tracks on the DLC coatings after the sliding wear tests (total distance of 43.2 m) at reciprocating frequencies 1 Hz, 6 Hz and 36 Hz: (a) DLC, (b) Si-DLC, and (c) W-DLC.

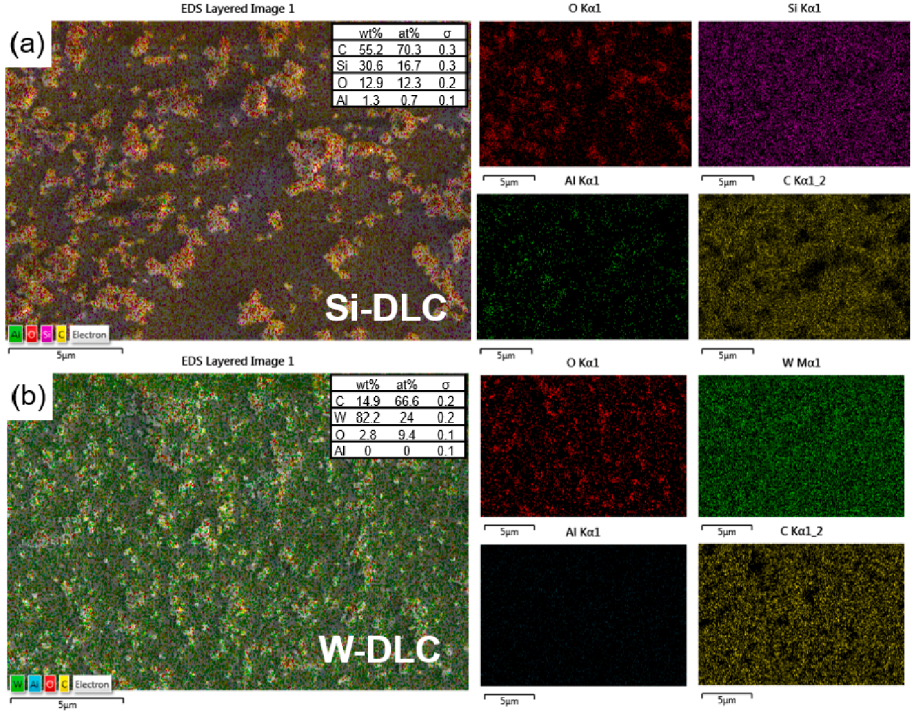

Fig. 12. EDX spectroscopy of the chemistry of wear debris adjacent to a 36 Hz reciprocating wear track on (a) Si-DLC and (b) W-DLC. For each coating, individual X-ray maps are shown for O K_α, Si K_α, Al K_α, W M_α, and C K_α X-rays adjacent to the normalised composite map (The chemistry tables at the right corners are these averaged over the whole scan area).

phase and structure of amorphous carbon or hydrocarbon molecules [28]. The peak intensity ratios between D and G bands (I(D)/I(G)) and wave number of G band peak positions are presented in Table 3, comparing the pristine as-fabricated DLC coatings with Raman spectra taken after the coatings were tested at 1 Hz, 6 Hz and 36 Hz. The increase of the peak intensity ratios (I(D)/I(G)), and the shifting of the

Table 3
Raman peak intensity I_D/I_G ratio and position of G band peak (cm^{-1}) measured on the surface of the DLC original coatings and in the wear tracks.

	Original surface		Wear track 1 Hz		Wear track 6 Hz		Wear track 36 Hz	
	I_D/I_G ratio	G band (cm^{-1})	I_D/I_G ratio	G band (cm^{-1})	I_D/I_G ratio	G band (cm^{-1})	I_D/I_G ratio	G band (cm^{-1})
DLC	0.52	1553	0.76	1563	0.75	1562	0.75	1564
Si-DLC	0.27	1502	0.26	1502	0.27	1503	0.26	1501
W-DLC	1.11	1563	1.20	1569	1.21	1570	1.21	1570

position of G band peak to a higher wave number on both non-doped DLC and W-DLC after wear tests, indicates a near-surface graphitization transformation from sp^3 to sp^2 bonds [29]. The I(D)/I(G) ratio and G peak position on the Si-DLC coatings remains unchanged at ~0.27 and ~1502 cm^{-1} indicating no detectable change in level of sp3 bonds.

Distinct from the DLC and W-DLC, the worn Si-DLC surface is dominated by a tribofilm of oxide-rich wear debris (Fig. 9), reducing the likelihood of surface graphitization. However, it is possible that a small degree of graphitization of the Si-DLC coatings occurs during the reciprocating contact when the tribofilm fractures exposing the fresh pristine Si-DLC surface underneath, particularly during stick-slip events (Fig. 5(b)).

4. Discussion

The friction and wear of DLC coatings are dependent on the DLC coatings' microstructure, surface morphology, chemical composition, mechanical properties and working conditions, and are influenced by complex tribological phenomena, such as adhesion, shearing, and abrasion [30]. Despite the wide use and outstanding mechanical and tribological properties of DLC coatings, there are still unclear aspects related to its self-lubricating properties, optimal chemical composition, and drawbacks when working under extreme conditions.

4.1. Doping effect on DLC mechanical properties

For the DLC, Si-DLC and W-DLC coatings investigated, a decrease of hardness and H/Er was observed in Si-DLC coatings (Fig. 4) that was due to the change in sp^3/sp^2 ratio compared to non-doped DLC. Si doping increases the Si–C (four-fold co-ordinated network) bridging bond and therefore weakens the adjacent C–C bond. This leads to an increase of the sp^3/sp^2 ratio because Si does not form π bond [3], which is consistent with the decrease of I(D)/I(G) ratio in Raman spectra from 0.52 to 0.27 after doping with Si (Table 3). For Si doped DLC, the coating hardness decreases with the content of Si from 16 GPa down to 12 GPa, as measured from dynamic indentation tests, corresponding to a Si content ranging from 0 to 3 % [31]. It has been shown that 1 %–2 % of Si doping is suitable for improving the adhesion of film and reducing internal stress while maintaining the surface hardness of DLC film with 15–16 GPa, which is close to the 16 GPa hardness of the Si-doped DLC coatings as measured in this study.

For W-doped DLC, the hardness also decreases with respect to non-doped DLC, due to the decrease of sp^3/sp^2 ratio consistent with the increase of I(D)/I(G) ratio in Raman spectra from 0.52 to 1.11 (Table 3). The 13 GPa W-DLC hardness measured in this study was slightly higher than those reported in Vengudusamy et al. [27] who reported 11–12 GPa on DLC doped with 12–21 at% W. Reducing W content up to 3.1 % can greatly improve the coating toughness and the adhesion with the substrate [32]. W contents >3.1 % can result in metallic W and WC phases in the DLC coatings [32], which were not detected here (Fig. 2).

4.2. Effect of sliding velocity on friction

Previous studies have only reported a decreasing trend of COF with higher sliding velocity for dry sliding tests of DLC coatings [33,34], interpreted as resulting from the graphitization process, i.e., the surface transformation from sp^3 to sp^2 bonds. The graphitization temperature of hydrogenated DLC coatings is normally within the range of 400–500 °C [35], which is caused by the hydrogen release from sp^3 bonds. The degree of graphite-like transformation increases with temperature [35], and the approximate rise in flash temperature at the contact interface due to sliding friction can be estimated based on a simple model for surface asperity [36].

$$\Delta T = \frac{\mu P v}{4a(K_1 + K_2)}, \left(a = \frac{P}{\pi H}\right) \quad (1)$$

where ΔT is the induced temperature rise, μ is the COF, P is the applied normal load, v is the sliding velocity, K_1 and K_2 are the thermal conductivities of the coating and the ball, respectively, a is the contact radius of the real contact area, and H is the measured coating hardness.

According to Equation (1), the contact interface temperature increases with higher sliding velocity; and which can therefore enhance the graphitization rate. The local heating effect will also be accentuated by dry reciprocating wear tests. This prediction agrees well with the observed graphitization and decrease in COF with increased sliding velocity behaviour of non-doped and W-doped DLC (Table 3 and Fig. 6). However, this graphitization-driven friction mechanism is not consistent with the behaviour of Si-doped DLC in this study, in which a significant increase of COF is observed at the highest velocity of 36 Hz (Fig. 6) and no graphitization was detected by Raman (Table 3). The increase in frictional-driven contact interface temperature due to higher sliding velocity is associated in Si-DLC with an increase in surface oxidative debris (Fig. 9), indicating a different wear mechanism.

For Si-DLC, in addition to an increase in COF with sliding velocity, severe fluctuations of the values of COF occurred within every few hundreds of cycles at the higher sliding velocities (6 Hz and 36 Hz, Fig. 5 (b)), with the formation of noticeably more wear debris comprising Si-rich and Al-rich oxide (from the counter-body) (Fig. 9). The severe fluctuation in COF of Si-DLC has been seen previously for Si-DLC [37,38], and attributed to the chemical interactions with counter-faces and gaseous molecules in their surroundings, which may form $SiO_x(OH)_y$ gel that could be adhesive that could lead to a higher friction [39]. Here, the significant fluctuations in Si-DLC COF (Fig. 6) occurring at higher sliding velocities are likely indicative of increased interfacial adhesion between the Al–Si surface oxides, and the tribo-surface of the Al_2O_3 counter-face ball. High interfacial adhesion can result in stick-slip events, together with shear, fracture and pull away of surface tribofilms, all of which can result in significant transitory increases in friction, formation of interfacial third-body particles, and wear.

4.3. Effect of sliding velocity on DLC wear

For the DLC, Si-DLC and W-DLC coatings and reciprocating wear tests evaluated, it was observed that the Si-DLC and W-DLC had significantly higher wear rates than the DLC (Fig. 7). The doped coatings have lower hardness than the DLC (Fig. 4), and their propensity to form brittle surface oxides under ambient testing conditions (Fig. 12) modifies their wear mechanism and wear rate. It was observed here that the wear debris of the Si-DLC and W-DLC worn against Al_2O_3 had significant oxide component (Fig. 12), consistent with enhanced wear.

The wear rate of the Si-DLC and W-DLC increased with sliding frequency (Fig. 7), with the W-DLC wear rate peaking at 6 Hz. At higher sliding velocities, and under reciprocating conditions, the temperature

at contact asperities increases. Higher surface temperatures will reduce local asperity hardness, increase the rate of DLC graphitization/hydrogen loss, and increase the rate of surface oxidization/tribofilm formation, all of which can increase wear rate.

A reduction of W-DLC wear rate at the highest sliding velocity 36 Hz (Fig. 7), similarly to what was observed for DLC by Kim [32], may be due to the formation of a thicker, protective tribofilm containing increased graphitic carbon. For a constant normal load, at lower sliding velocities tribofilms may be thin/not well formed [34], and thus easily displaced by the reciprocating ball. However, at high velocity, and increased surface temperature, the faster build-up of a thicker tribofilm can act as a protective mechanism, reducing subsequent wear rate as observed for the W-DLC here (Fig. 7). The reduction in wear rate of W-DLC at high frequency (36 Hz) via a stable tribofilm containing graphitic carbon (Table 3) also correlates with the observed reduction in COF (Fig. 6) at higher sliding velocities. In contrast, the Si-DLC exhibits a progressive increase in wear rate, which by 36 Hz is larger than the W-DLC (Fig. 7). This correlates with the dominance of oxidative friction and wear processes of the Si-DLC coating, and no detectable formation of graphitic carbon in the surface tribofilm (Table 3).

5. Conclusions

The friction and wear behaviour of non-doped, Si-doped, and W-doped DLC coatings, have been evaluated by reciprocating dry sliding tests at three reciprocating frequencies 1 Hz, 6 Hz and 36 Hz. Three key conclusions are:

1. Si-doped DLC has the lowest surface roughness and initially exhibits a lower COF than DLC and W-DLC at low frequencies of 1 Hz and 6 Hz. However, at 6 Hz and 36 Hz, Si-DLC exhibits significant fluctuations in COF with the highest COF at 36 Hz, the opposite trend to non-doped and W-doped DLC whose COF systematically drop with increased sliding velocity.
2. Si-DLC friction and wear is dominated by oxidative mechanisms, which degrade performance at higher sliding velocities. Significant amounts of wear debris were observed on the Si-doped DLC post-test, comprising mainly Si-rich and Al-rich oxide (from the Alumina ball). The oxide-rich tribofilm, and lack of surface graphitization, result in severe fluctuations of Si-DLC friction via stick-slip and surface fracture/wear mechanisms, and significantly increased COF and wear rate during the sliding tests at higher 6 Hz and 36 Hz reciprocating frequencies.
3. Higher velocities increase the local surface temperature at the tribocontact region leading to increased surface graphitization of DLC and W-DLC and resulting in decreased COF. The surface oxidised W-DLC coatings exhibited a significant increase in wear rate at intermediate sliding velocity (6 Hz), however the wear rate reduced at high sliding velocity (36 Hz) due to a more resistant protective tribofilm containing graphitic carbon with a low COF.

Declaration of competing interest

The authors declare that they have no known competing financial interests or personal relationships that could have appeared to influence the work reported in this paper.

Acknowledgement

This work is supported by the Engineering and Physical Sciences Research Council (Grant number EP/R001766/1) as a part of 'Friction: The Tribology Enigma' (www.friction.org.uk), a collaborative Programme Grant between the Universities of Leeds and Sheffield.

References

[1] C. Donnet, A. Erdemir, Solid lubricant coatings: recent developments and future trends, Tribol. Lett. 17 (3) (2004) 389–397.
[2] A. Tyagi, R. Walia, Q. Murtaza, S.M. Pandey, P.K. Tyagi, B. Bajaj, H. Materials, A critical review of diamond like carbon coating for wear resistance applications, Int. J. Refract. Metals Hard Mater. 78 (2019) 107–122.
[3] R. Zahid, H.H. Masjuki, M. Varman, M.A. Kalam, R.A. Mufti, N.W.B.M. Zulkifli, M. Gulzar, S.S.B.N. Azman, Influence of intrinsic and extrinsic conditions on the tribological characteristics of diamond-like carbon coatings: A Review, J. Mater. Res. 31 (13) (2016) 1814–1836.
[4] A. Erdemir, The role of hydrogen in tribological properties of diamond-like carbon films, Surf. Coating. Technol. 146 (2001) 292–297.
[5] W.H. Kao, Optimized a-C : W-x% coatings with enhanced tribological properties and improved micro-drilling performance, Surf. Coating. Technol. 201 (16–17) (2007) 7392–7400.
[6] Y. Wang, Y. Ye, H. Li, L. Ji, Y. Wang, X. Liu, J. Chen, H. Zhou, Microstructure and tribological properties of the a-C:H films deposited by magnetron sputtering with CH4/Ar mixture, Surf. Coating. Technol. 205 (19) (2011) 4577–4581.
[7] A.A. Voevodin, S.D. Walck, J.S. Zabinski, Architecture of multilayer nanocomposite coatings with super-hard diamond-like carbon layers for wear protection at high contact loads, Wear 203 (1997) 516–527.
[8] Y.L. Su, W.H. Kao, Effect of thickness and carbon content on tribological behaviour and mechanical properties of Ti-C : H coatings, Wear 236 (1–2) (1999) 221–234.
[9] L.F. Xia, Z.H. Yan, J.X. Liao, Effects of intermediate layers on the tribological behavior of DLC coated 2024 aluminum alloy, Wear 257 (5–6) (2004) 599–605.
[10] J.-H. Ouyang, S. Sasaki, J. Murakami, Y. Zhou, J. Zhang, Mechanical and unlubricated tribological properties of titanium-containing diamond-like carbon coatings, Wear 266 (1–2) (2009) 96–102.
[11] X. Chen, Z. Peng, Z. Fu, S. Wu, W. Yue, C. Wang, Microstructural, mechanical and tribological properties of tungsten-gradually doped diamond-like carbon films with functionally graded interlayers, Surf. Coating. Technol. 205 (12) (2011) 3631–3638.
[12] L. Wang, S. Wan, S.C. Wang, R.J.K. Wood, Q.J. Xue, Gradient DLC-based nanocomposite coatings as a solution to improve tribological performance of aluminum alloy, Tribol. Lett. 38 (2) (2010) 155–160.
[13] S.C. Ray, W. Pong, P.J.T.S.F. Papakonstantinou, Iron, nitrogen and silicon doped diamond like carbon, DLC) thin films: a comparative study 610 (2016) 42–47.
[14] S. Akaike, D. Kobayashi, Y. Aono, M. Hiratsuka, A. Hirata, T. Hayakawa, Y.J. D. Nakamura, R. Materials, Relationship between static friction and surface wettability of orthodontic brackets coated with diamond-like carbon (DLC), fluorine-or silicone-doped DLC coatings 61 (2016) 109–114.
[15] M. Kalin, J. Vizintin, Differences in the tribological mechanisms when using non-doped, metal-doped (Ti, WC), and non-metal-doped (Si) diamond-like carbon against steel under boundary lubrication, with and without oil additives, Thin Solid Films 515 (4) (2006) 2734–2747.
[16] M.G. Kim, K.R. Lee, K.Y. Eun, Tribological behavior of silicon-incorporated diamond-like carbon films, Surf. Coating. Technol. 112 (1–3) (1999) 204–209.
[17] D.-C. Pham, H.-S. Ahn, J.-E. Oh, E.-S. Yoon, Tribochemical interactions of Si-doped DLC film against steel in sliding contact, J. Mech. Sci. Technol. 21 (7) (2007) 1083–1089.
[18] K. Oguri, T. Arai, 2 different low friction mechanisms OF diamond-like carbon with silicon coatings formed BY plasma-assisted chemical vapor-deposition, J. Mater. Res. 7 (6) (1992) 1313–1316.
[19] R. Gilmore, R. Hauert, Comparative study of the tribological moisture sensitivity of Si-free and Si-containing diamond-like carbon films, Surf. Coating. Technol. 133 (2000) 437–442.
[20] T. Iseki, H. Mori, H. Hasegawa, H. Tachikawa, K. Nakanishi, Structural analysis of Si-containing diamond-like carbon, Diam. Relat. Mater. 15 (4–8) (2006) 1004–1010.
[21] J. Ando, T. Ohmori, A. Murase, N. Takahashi, T. Yamaguchi, K. Hokkirigawa, Tribological properties of Si-containing diamond-like carbon film under ATF lubricated condition, Wear 266 (1–2) (2009) 239–247.
[22] M. Ban, M. Ryoji, S. Fujii, J. Fujioka, Tribological characteristics of Si-containing diamond-like carbon films under oil-lubrication, Wear 253 (3–4) (2002) 331–338.
[23] T. Yamaguchi, J. Ando, T. Tsuda, N. Takahashi, M. Tohyama, A. Murase, T. Ohmori, K. Hokkirigawa, Sliding velocity dependency of the friction coefficient of Si-containing diamond-like carbon film under oil lubricated condition, Tribol. Int. 44 (11) (2011) 1296–1303.
[24] J. Lanigan, H. Zhao, A. Morina, A. Neville, Tribochemistry of silicon and oxygen doped, hydrogenated Diamond-like Carbon in fully-formulated oil against low additive oil, Tribol. Int. 82 (2015) 431–442.
[25] J.L. Lanigan, C. Wang, A. Morina, A. Neville, Repressing oxidative wear within Si doped DLCs, Tribol. Int. 93 (2016) 651–659.
[26] L. Yang, A. Neville, A. Brown, P. Ransom, A. Morina, Friction reduction mechanisms in boundary lubricated W-doped DLC coatings, Tribol. Int. 70 (2014) 26–33.
[27] B. Vengudusamy, J.H. Green, G.D. Lamb, H.A. Spikes, Tribological properties of tribofilms formed from ZDDP in DLC/DLC and DLC/steel contacts, Tribol. Int. 44 (2) (2011) 165–174.
[28] A.C. Ferrari, J.C. Meyer, V. Scardaci, C. Casiraghi, M. Lazzeri, F. Mauri, S. Piscanec, D. Jiang, K.S. Novoselov, S. Roth, A.K. Geim, Raman spectrum of graphene and graphene layers, Phys. Rev. Lett. 97 (18) (2006).
[29] T. Fc, T.J.M.t. Sl, Correlation between ID/IG ratio from visible Raman spectra and sp2/sp3 ratio from XPS spectra of annealed hydrogenated DLC film 47 (7) (2006) 1847–1852.

[30] A.J.S. Grill, C. Technology, Tribology of diamondlike carbon and related materials: an updated review 94 (1997) 507–513.
[31] M. Ikeyama, S. Nakao, Y. Miyagawa, S. Miyagawa, Effects of Si content in DLC films on their friction and wear properties, Surf. Coating. Technol. 191 (1) (2005) 38–42.
[32] Z.-q. Fu, C.-b. Wang, W. Zhang, W. Wang, W. Yue, X. Yu, Z.-j. Peng, S.-s. Lin, M.-j. Dai, Influence of W content on tribological performance of W-doped diamond-like carbon coatings under dry friction and polyalpha olefin lubrication conditions, Mater. Des. 51 (2013) 775–779.
[33] D.-W. Kim, K.-W. Kim, Effects of sliding velocity and normal load on friction and wear characteristics of multi-layered diamond-like carbon (DLC) coating prepared by reactive sputtering, Wear 297 (1) (2013) 722–730.
[34] K. Al Mahmud, M.A. Kalam, H.H. Masjuki, H. Mobarak, N. Zulkifli, An updated overview of diamond-like carbon coating in tribology, Crit. Rev. Solid State Mater. Sci. 40 (2) (2015) 90–118.
[35] T. Le Huu, H. Zaidi, D. Paulmier, P. Voumard, Transformation of sp3 to sp2 sites of diamond like carbon coatings during friction in vacuum and under water vapour environment, Thin Solid Films 290 (1996) 126–130.
[36] Z. Zhou, K. Li, I. Bello, C. Lee, S. Lee, Study of tribological performance of ECR–CVD diamond-like carbon coatings on steel substrates: Part 2. The analysis of wear mechanism, Wear 258 (10) (2005) 1589–1599.
[37] C. Donnet, M. Belin, J. Auge, J. Martin, A. Grill, V. Patel, Tribochemistry of diamond-like carbon coatings in various environments, Surf. Coating. Technol. 68 (1994) 626–631.
[38] A. Erdemir, M. Switala, R. Wei, P. Wilbur, A tribological investigation of the graphite-to-diamond-like behavior of amorphous carbon films ion beam deposited on ceramic substrates, Surf. Coating. Technol. 50 (1) (1991) 17–23.
[39] X. Wu, T. Ohana, A. Tanaka, T. Kubo, H. Nanao, I. Minami, S. Mori, Tribochemical reaction of Si-DLC coating in water studied by stable isotopic tracer, Diam. Relat. Mater. 17 (2) (2008) 147–153.